Benchmarking Transient Natural Convection In An Enclosure

D. T. Reindl, W. A. Beckman, J. W. Mitchell, C. J. Rutland
University of Wisconsin - Madison
Department of Mechanical Engineering

Abstract

An insulated square cavity enclosing an isothermal vertical flat plate is proposed as a suitable geometry for validating codes and algorithms capable of computing solutions to the transient Navier-Stokes and energy equations. The vertical flat plate in the enclosure is very thin and located in the center of the cavity which permits assumptions of symmetry. The relative length of the plate is half that of the side of the enclosing cavity. Initially, the cavity contains a quiescent isothermal fluid. At time zero, a step change in plate temperature begins to influence the internal flow. The final condition in the cavity is a quiescent isothermal fluid at a temperature equal to the plate temperature. (An advantage of this configuration is the unambiguous initial and final conditions.)

The problem is solved using a finite element computer code FIDAP [6]. Benchmark solutions are obtained for $10^3 \le Ra \le 10^6$. Specific quantities of interest include: average Nusselt number over time, maximum x and y components of velocity (maximum over all time), and maximum stream function (maximum over all time). The heat transfer results compare well with limiting cases.

Nomenclature

$\overline{F}$	Vector of forcing functions
g	Acceleration due to gravity (m^2/s)
h	Mesh size parameter (smallest element size)
H	Rectangular cavity height (m)
$\overline{K}$	Combined momentum and thermal diffusion matrix
L	Flat plate length (m)
$\overline{M}$	Combined mass and capacitance matrix
n	Normal directed unit vector
$\overline{Nu}$	Average Nusselt number (Eq. 5)
P	Pressure (N/m^2)
Pr	Prandtl number (ν/α)
Ra	Rayleigh number ($g\beta L^3\Delta T/\nu\alpha$)
t	Time (s)
T	Temperature (C)
u	x-component of velocity (m/s)
U	Characteristic velocity (m/s)
v	y-component of velocity (m/s)
V	Vector of nodal unknown velocities and temperatures
W	Rectangular cavity width (m)
x	x-coordinate distance (m)
y	y-coordinate distance (m)

Greek Symbols:

β	Volume expansion coefficient (1/C)
ΔT	Initial temperature difference (T_w-T_o) (C)
γ	Time truncation error tolerance
ϵ	Penalty parameter, (1E-8)
ρ	Density (kg/m^3)
ψ	Stream function

Subscripts:

max	Maximum over time of a dimensionless quantity
o	Initial value
w	Wall

Superscripts:

$\cdot$	Dimensionless quantity

1 Introduction

The simplest and one of the most comprehensively studied enclosure problems is the steady state solution of a two dimensional rectangular cavity with differentially heated side walls and adiabatic top and bottom. Jones [1] suggested that this problem would be suitable for validating and testing new computer codes and numerical techniques. This prompted a large scale computational comparison exercise by de Vahl Davis and Jones [2]. Thirty contributors submitted solutions to the cavity problem with a unity aspect ratio and $10^3 \le Ra \le 10^6$. Various calculated and derived quantities e.g. max stream function, velocity components, etc were selected to be included in the comparison. In an attempt to determine the "true" solution, de Vahl Davis [3] solved a stream function - vorticity formulation using refined grids ($11 \times 11 \rightarrow 81 \times 81$ uniform meshes) and Richardson extrapolation. This problem continues to be used as a basis for testing new codes and numerical techniques.

As a preface to this work, the steady state differentially heated square cavity problem was solved with the code used in the current work (FIDAP). A graded mesh of 30x30 elements yielded excellent agreement with the de Vahl Davis benchmark solution (e.g. $\overline{Nu}$ results were within 0.33% of de Vahl Davis over the range of Ra). Although the current geometry and conditions differ considerably from the differentially heated cavity, agreement with the de Vahl Davis benchmark lends some level of confidence in the ability of the code to model coupled flows.

2 Problem Definition

The existing benchmark problem of the differentially heated square cavity only considers steady state analysis with the bounding walls being responsible for "driving" the flow. A number of relevant applications are time dependent and contain sources within an enclosure which are responsible for driving the natural convection flow. For example, printed circuit boards with electronic devices generating heat are responsible for driving the flows in many electronic packaging configurations. Another example is found in thermal storage tanks with energy being transferred to the tank storage medium via immersed heat exchangers. These applications dictate the need for analyzing natural convection in an enclosure that contains sources. This type of configuration would also be suitable as a test problem for codes capable of computing transient fluid flow and energy transfer.

One of the simplest transient enclosure problems containing a source is an insulated rectangular cavity with a heated vertical flat plate on the interior as shown in Fig. 1.

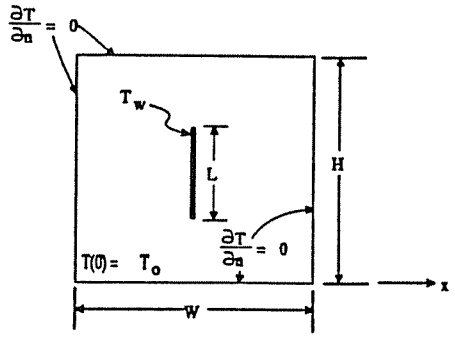

Fig. 1 : Adiabatic cavity with a heated vertical plate source.

Khalilollahi and Sammakia [4] considered the problem of a vertical flat plate (of height $H/3$) centered in an adiabatic cavity. The overall aspect ratio (H/W) of the cavity was 0.25 and the Rayleigh number was fixed at $Ra = 3.35 \times 10^6$. The authors noted the existence of three temporal regimes. Initially the behavior is dominated by pure conduction followed by a brief convective regime which closely agrees with the behavior of a flat plate in an infinite medium. At later times the flow field decays as the bulk temperature in the cavity rises.

The benchmark problem proposed here is same as that shown in Fig. 1. The height of the unit aspect ratio enclosure is assumed to be twice the vertical plate length L (H=W=2L). The vertical plate is centered inside the cavity and the Rayleigh number (based on the plate length L and initial temperature difference $\{T_w - T_o\}$ will be varied from $10^3 \le Ra \le 10^6$. The quantities of interest include: average heat flux from plate (average Nusselt number), maximum x and y components of velocity (maximum over all time), and maximum stream function (maximum over all time). The working fluid has constant properties with Pr=3.57.

3 Mathematical Formulation and Solution Technique

Assuming the plate in the square enclosure is infinitely thin and located in the center of the cavity i.e. at x=$W/2$, symmetry can be used to reduce the computational domain in half as shown in Fig. 2.

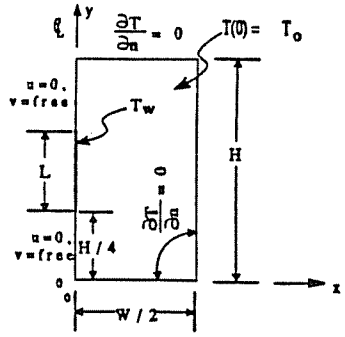

Fig. 2 : Computational domain for the enclosure with a flat plate.

It is convenient to non-dimensionalize the governing system of equations with the variables given in Table 1.

$x^* = x/L$	$y^* = y/L$
$u^* = u/U$	$v^* = v/U$
$T^* = (T - T_o)/(T_w - T_o)$	$P^* = P/\rho U^2$
$t^* = tU/L$	$U = \sqrt{g\beta(T_w - T_o)L}$

Table 1 : Variable Non-dimensionalization.

The Boussinesq approximation is used to relate the force term (buoyancy force) to temperature. Gray and Giorgini [5] develop and investigate the validity of the approximation. The essence of the approximation consists of the following: density is assumed constant except in the momentum body force terms, all other properties are assumed constant, viscous dissipation is negligible. Based on the above assumptions, the dimensionless governing equations (dropping the * superscript) and boundary conditions are:

Conservation of Mass:

$$\frac{\partial u}{\partial x} + \frac{\partial v}{\partial y} = 0 \tag{1}$$

x - Momentum:

$$\sqrt{\frac{Ra}{Pr}}\left[\frac{\partial u}{\partial t} + u\frac{\partial u}{\partial x} + v\frac{\partial u}{\partial y} + \frac{\partial P}{\partial x}\right] = \frac{\partial^2 u}{\partial x^2} + \frac{\partial^2 u}{\partial y^2} \tag{2}$$

y - Momentum:

$$\sqrt{\frac{Ra}{Pr}}\left[\frac{\partial v}{\partial t} + u\frac{\partial v}{\partial x} + v\frac{\partial v}{\partial y} + \frac{\partial P}{\partial y}\right] = \frac{\partial^2 v}{\partial x^2} + \frac{\partial^2 v}{\partial y^2} + \sqrt{\frac{Ra}{Pr}}T \tag{3}$$

Energy:

$$\sqrt{RaPr}\left[\frac{\partial T}{\partial t} + u\frac{\partial T}{\partial x} + v\frac{\partial T}{\partial y}\right] = \frac{\partial^2 T}{\partial x^2} + \frac{\partial^2 T}{\partial y^2} \tag{4}$$

Boundary Conditions:

@ $x = 0$	$0 \le y < 0.5$	$u = 0, \partial v/\partial x = 0$	$\partial T/\partial n = 0$
@ $x = 0$	$1.5 < y \le 2$	$u = 0, \partial v/\partial x = 0$	$\partial T/\partial n = 0$
@ $x = 0$	$0.5 \le y \le 1.5$	$u = v = 0$	$T = T_w = 1$
@ $x = 1$	$0 \le y \le 2$	$u = v = 0$	$\partial T/\partial n = 0$
@ $y = 0$	$0 \le x \le 1$	$u = v = 0$	$\partial T/\partial n = 0$
@ $y = 2$	$0 \le x \le 1$	$u = v = 0$	$\partial T/\partial n = 0$

Initial Conditions:

for all x and y	$u = v = 0$	$T(0) = T_o = 0$

A quantity of primary interest in this study is the average Nusselt number (average dimensionless heat flux) $\overline{Nu}$ over the plate. The average Nusselt number is the integral of the local heat flux over the length of the vertical plate as given by

$$\overline{Nu} = \int_0^1 \frac{\partial T}{\partial x}\Big|_{wall}\, dy \qquad (5)$$

The governing partial differential equations given by Eq. 1-4 are solved in primitive variable form with FIDAP [6] using a Galerkin finite element approximation. The penalty function approach is used to approximate pressure in the primitive variable formulation. The penalty method relaxes the strict continuity requirement by letting

$$\frac{\partial u}{\partial x} + \frac{\partial v}{\partial y} = -\varepsilon P \qquad (6)$$

where ε is a penalty parameter ($\varepsilon \sim 10^{-5} - 10^{-9}$). Solving Eq. 6 for pressure and substituting the result into Eq. 2 and 3 eliminates pressure from the system. The pressure can be obtained subsequently by postprocessing $P = -[\partial u/\partial x + \partial v/\partial y]/\varepsilon$. For further discussion of the penalty method, see Sani, et al. [7].

The elements are nine node quadrilaterals with a quadratic basis for velocity and temperature. Element integrals are performed numerically using a third order Gaussian quadrature.

Upon applying the finite element approximations (Galerkin optimizing criteria, basis function selection, etc.), the system of partial differential equations (Eq. 1-4) are transformed into a discrete set of ordinary differential equations as given by

$$\overline{M}\frac{dV}{dt} + \overline{K}(V)V = \overline{F} \qquad (7)$$

where $\overline{M}$ is a combined mass and capacitance matrix, $\overline{K}$ is a combined momentum and thermal diffusion matrix, V is a vector of unknown nodal velocities and temperatures, and $\overline{F}$ is the vector of forcing functions. Eq. 7 represents a system of initial value problems for each of the nodal unknowns.

A second order implicit trapezoid rule multi-step scheme is used to integrate this system of equations. The first step (a predictor) is based on the Adams-Bashforth method with variable time increment as given by

$$V_{k+1}^p = V_k + \frac{\delta t_k}{2}\left\{\left(2 + \frac{\delta t_k}{\delta t_{k-1}}\right)\dot{V}_k - \frac{\delta t_k}{\delta t_{k-1}}\dot{V}_{k-1}\right\} \qquad (8)$$

where V_{k+1}^p is the predicted vector of unknowns at time $k+1$, $\dot{V}_k$ is the time rate change of the unknowns at time k, and δt_k is the time increment at step k. The second step (a corrector) is the trapezoid rule with a variable time increment. When applied to Eq. 7, the trapezoid rule yields

$$\overline{M}\frac{V_{k+1}^c - V_k}{\delta t_k} + \frac{1}{2}\{\overline{K}(V_{k+1}^c)V_{k+1}^c + \overline{K}(V_k)V_k\} = \frac{1}{2}\{\overline{F}_{k+1} + \overline{F}_k\} \qquad (9)$$

The acceleration vectors $\dot{V}$ in Eq. 8 and 9 are computed recursively from the definition of the trapezoid rule by

$$\dot{V}_{k+1} = \frac{2}{\delta t_k}\{V_{k+1} - V_k\} - \dot{V}_k \qquad (10)$$

where $\dot{V}_k$ is found from the previous use of Eq. 10.

The above two step time integration scheme is able to accommodate a variable step size time increment. If a fixed time increment is specified, further simplifications to the above scheme are possible. Although a fixed time increment would allow the use of Richardson extrapolation at each time step, the exorbitant computational resources required to carry out the time integration for the system of equations considered here precludes this approach. The authors have elected to use an adaptive time integration scheme. The adaptive scheme allows the time step to increase or decrease depending on the magnitude of the local time truncation error. The local time truncation error for the Adams-Bashforth method is

$$V_{k+1}^p - V(t_{k+1}) = -\frac{1}{12}\left(2 + 3\frac{\delta t_{k-1}}{\delta t_k}\right)\delta t_k^3 \ddot{V}_{k+1} + O(\delta t_k^4) \qquad (11)$$

Similarly, the local time truncation error for the trapezoid rule is given by

$$E_{k+1} = V_{k+1}^c - V(t_{k+1}) = \frac{1}{12}\delta t_k^3 \ddot{V}_{k+1} + O(\delta t_k^4) \qquad (12)$$

Combining Eq. 11 and 12 yields

$$E_{k+1} = \frac{V_{k+1}^c - V_{k+1}^p}{3\left(1 + \frac{\delta t_{k-1}}{\delta t_k}\right)} + O(\delta t_k^4) \qquad (13)$$

The result in Eq. 13 can be used to estimate the size of the next time step by requiring the relative norm of the error for the next step to be less than a specified tolerance ($\|E_{k+2}\| \le \gamma$). From Eq. 12, the following relationship for time truncation error results.

$$\frac{E_{k+2}}{E_{k+1}} = \left(\frac{\delta t_{k+1}}{\delta t_k}\right)^3 \frac{\ddot{V}_{k+2}}{\ddot{V}_{k+1}} \qquad (14)$$

By taking norms and using the fact $\ddot{V}_{k+2} = \ddot{V}_{k+1} + O(\delta t)$ as well as $\|E_{k+2}\| \le \gamma$, Eq. 14 results in an expression to determine the relative size of the next time increment.

$$\frac{\delta t_{k+1}}{\delta t_k} = \left(\frac{\gamma}{\|E_{k+1}\|}\right)^{1/3} \qquad (15)$$

where the norm $\|E_{k+1}\|$ is defined in Appendix A and higher order terms have been omitted. The time integration scheme results in a system of nonlinear algebraic equations to be solved at each time step. The system of nonlinear equations is solved by a quasi-Newton method.

4 Results

The results of computations performed for the proposed transient benchmark geometry shown in Fig. 2 are given in this section. First, spatial and temporal refinement techniques are employed to determine appropriate mesh densities for computing accurate solutions. Next, the Nusselt number results are compared with some limiting cases. Finally, solutions for Ra=10^3, 10^4, 10^5, and 10^6 are presented.

4.1 Mesh Refinement Results

The development of a "benchmark" solution demands careful consideration to spatial and temporal resolution to assure the final solutions are independent of the computational meshes (space and time). Ideally, an extrapolation scheme such as Richardson extrapolation would be applied to construct both the space and time accurate solutions. The adaptive time integration scheme creates difficulty in extrapolating solutions because the dependent variables are not necessarily known at the same times for various refined meshes. Thus, the mesh refinement process will be performed in two steps. First, spatial resolution will be performed to demonstrate a solution that is independent of the mesh. Second, time mesh refinement will be performed to determine an allowable level of time truncation error γ.

Since obtaining accurate solutions becomes more difficult as the Rayleigh number increases, mesh refinement will be performed on the $Ra=10^6$ case. Two quantities will be used as indicators of the effects of successive mesh refinement: $\overline{Nu}$ and the v-velocity. The v-velocity was selected since it is the dominant velocity component. The average Nusselt number for the 1299 element case is shown in Fig. 3. The relative differences in the average Nusselt number with respect to the finest mesh (1299 elements) for successively refinement meshes are shown in Fig. 4.

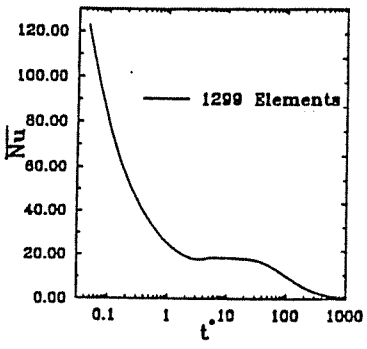

Fig. 3 : Transient $\overline{Nu}$ for 1299 Elements, $Ra=10^6$.

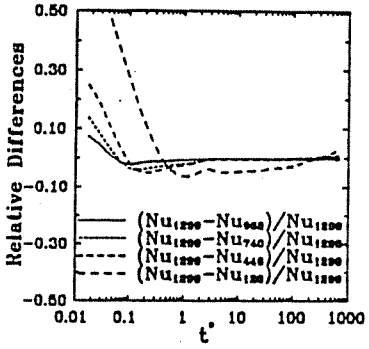

Fig. 4 : Relative difference in $\overline{Nu}$ with respect to 1299 element mesh for 120, 449, 740, and 968 element meshes, $Ra=10^6$.

The relative differences in the average Nusselt number become very small for the 740 and 968 element cases. Thus, it is appears that the temperature solution is mesh independent when the 740 element level is reached. (A measure of the mesh size for 740 element case is $h=0.007051$ and for 1299 elements $h=0.004892$.) Next, the distribution of dimensionless v-velocities across the width of the cavity are plotted at three vertical heights (1/3, 2/3 from plate bottom and top of plate) for a time in which the velocities are near their peak values.

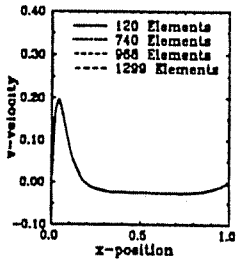

Fig. 5 : v^* velocity at $y^*=0.83$, $t^*=5.0$, $Ra=10^6$.

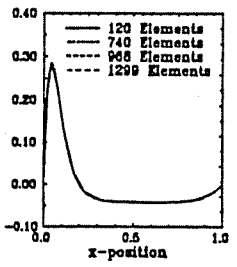

Fig. 6 : v^* velocity at $y^*=1.167$, $t^*=5.0$, $Ra=10^6$.

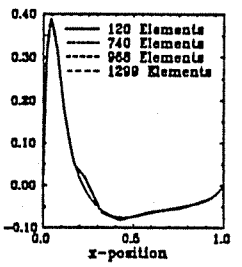

Fig. 7 : v^* velocity at $y^*=1.50$, $t^*=5.0$, $Ra=10^6$.

The velocities are essentially identical for mesh densities greater than 740 elements. Since the 740 element mesh provides an acceptable level of spatial resolution of both velocities and temperature, it will used to compute the final benchmark solution for this problem. The 740 element mesh is shown below in Fig. 8a along with the 1299 element mesh in Fig. 8b.

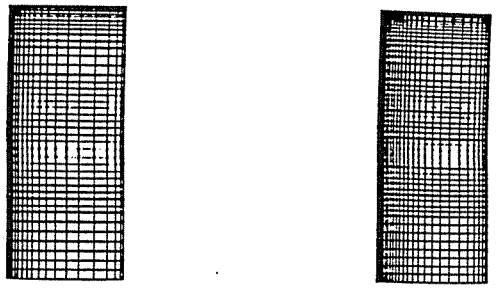

(a) (b)

Fig. 8 : Mesh for square cavity with a heated vertical flat plate; (a) 740 elemen (b) 1299 elements.

Temporal refinement was performed by varying the tolerance o the local truncation error of the time integration scheme γ an observing the effect on the magnitude and time in which the pea values of dimensionless u and v velocities and stream function $|\psi|_m$ occur. The temporal refinement results are given below

γ	u_{max}	t^*	v_{max}	t^*	$\lvert\psi\rvert_{max}$	t^*
0.005	0.4003	5.51	0.5382	4.40	0.0545	5.51
0.003	0.4038	5.89	0.5368	4.95	0.0548	5.51
0.001	0.4018	5.52	0.5364	4.99	0.0556	5.52
0.0005	0.4022	5.66	0.5373	5.03	0.0559	5.49
0.0001	0.4025	5.58	0.5381	5.03	0.0559	5.48
0.00005	0.4025	5.60	0.5381	5.01	0.0558	5.52

Table 2 : Temporal refinement results, $Ra=10^6$, 740 element mesh

The results from Table 2 indicate that the maximum velocities an stream function have converged and a tolerance of $\gamma=0.000$ th local truncation error will yield time accurate solutions. Thus, th mesh shown in Fig. 8 and a tolerance of $\gamma=0.0001$ on the tim truncation error will be used for computing the final benchmar solution.

4.2 Limiting Cases

The mesh refinement techniques performed in the previou section attempted to determine spatial and temporal mesh densitie which yield accurate solutions. There are two additional comparison that can be made to lend confidence to the solutions. The heat transfe results can be compared with two limiting cases: pure conduction an natural convection from a vertical flat plate in an infinite medium The analytical solution to the one-dimensional transient pur conduction problem is compared with the numerical solution in Fig 9.

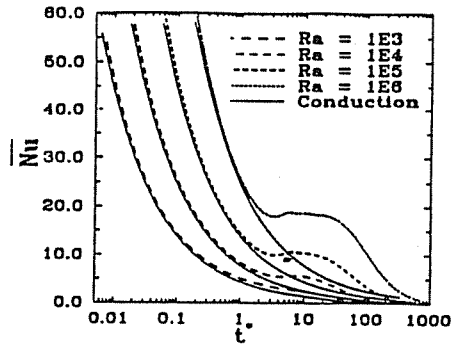

Fig. 9 : Transient $\overline{Nu}$ for the complete range of Rayleigh numbers including one-dimensional pure conduction solutions.

The respective one-dimensional conduction solutions are given by the solid lines. The agreement between the computed solution and the analytical solution is very good during the early conduction dominated regime. The computed solutions compared with the steady state infinite medium solutions are shown below in Fig. 10.

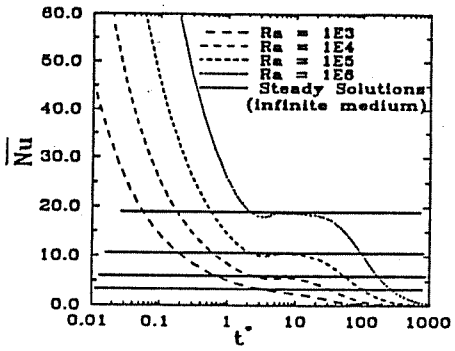

Fig. 10 : Transient $\overline{Nu}$ for a range of Rayleigh numbers including infinite medium solutions.

The solid lines are the heat transfer results for a vertical flat plate in an infinite medium as given by Churchill and Chu [8]. Reasonable agreement for each Rayleigh number case is obtained during a short quasi-steady period.

4.3 The Benchmark Solution

Time dependent benchmark problems present unique difficulties in selecting useful and appropriate quantities to present for comparison. Because the amount of data generated in the time dependent computation of this problem is immense, only selected quantities which characterize the heat transfer and fluid flow aspects of this problem will be presented graphically. Tabular results for three positions in the cavity at t^*=5.0 are given in Appendix B.

Table 3 presents the benchmark results for the velocity components and stream function ψ. Included in the table are the maximum magnitudes of the respective variables, the time at which the maximum occurs as well as the x-y location (nodal maximum i.e. without spatial interpolation) of the maximum.

Ra	u_{max}	t^*	x^*	y^*	v_{max}	t^*	x^*	y^*	$\lvert\psi\rvert_{max}$	t^*	x^*	y^*
10^3	0.0716	6.68	0.465	1.748	0.1220	5.71	0.174	1.100	0.03546	5.71	0.419	1.10
10^4	0.1965	6.22	0.419	1.812	0.2706	5.76	0.135	1.350	0.07075	6.22	0.419	1.35
10^5	0.3059	5.54	0.309	1.881	0.3843	5.36	0.000	1.697	0.07233	5.94	0.342	1.57
10^6	0.4025	5.58	0.174	1.946	0.5381	5.03	0.000	1.748	0.05591	5.48	0.276	1.69

Table 3 : Benchmark solution results, 740 element mesh, $\gamma = 0.0001$.

The benchmark $\overline{Nu}$ results are shown in both Figs. 9 and 10.

In addition to the above benchmark solutions, contours of v, T, and ψ at time t^*=5.0 for the complete range of Rayleigh number are given in Figs. 11-14.

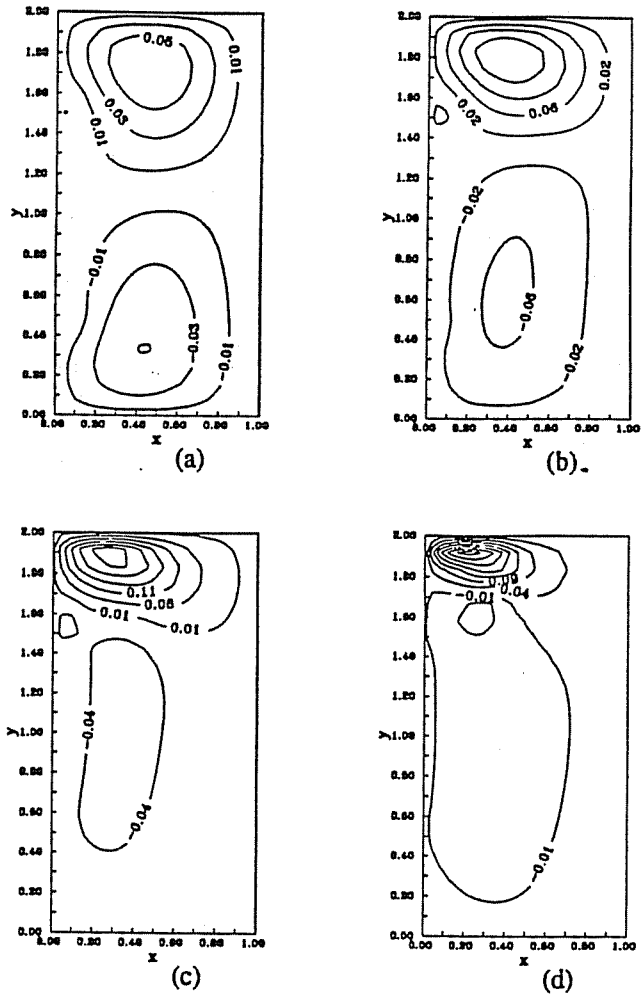

Fig. 11 : Contour maps of u velocity at t^*=5.0: (a) Ra=10^3, $u_{min} = -0.05$, $\Delta u = 0.02$, $u_{max} = 0.06$ i.e., -0.05(0.02)0.06; (b) Ra=10^4, -0.06(0.04)0.16; (c) Ra=10^5, -0.04(0.05)0.28; (d) Ra=10^6, -0.06(0.05)0.36.

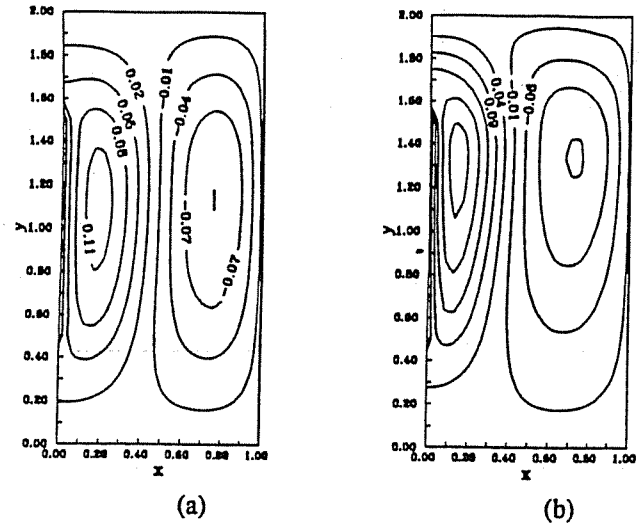

Fig. 12 : Contour maps of v velocity at t^*=5.0: (a) Ra=10^3, $v_{min} = -0.1$, $\Delta v = 0.03$, $v_{max} = 0.12$ i.e., -0.1(0.03)0.12; (b) Ra=10^4, -0.16(0.05)0.26; (c) Ra=10^5, -0.12(0.07)0.36; (d) Ra=10^6, -0.16(0.07)0.52.

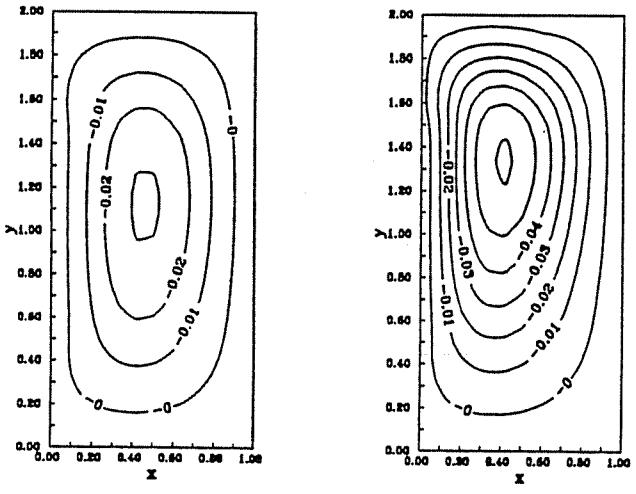

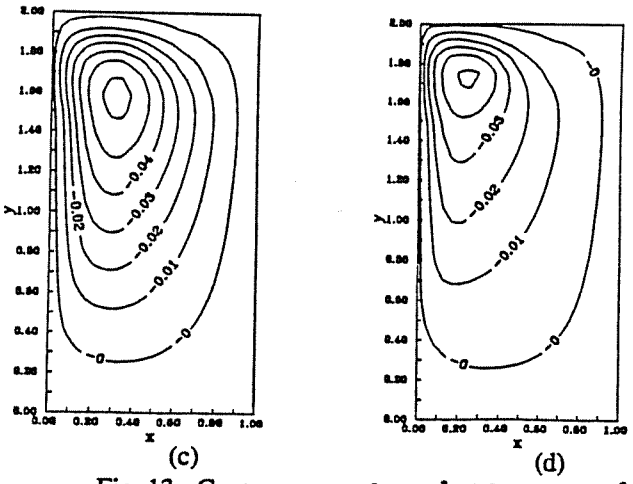

Fig. 13 : Contour maps of ψ at t^*=5.0: (a) Ra=10^3, $\psi_{min} = -0.034$, $\Delta\psi = 0.01$, $\psi_{max} = 0.0$ i.e., -0.034(0.01)0.0; (b) Ra=10^4, -0.064(0.01)0.0; (c) Ra=10^5, -0.064(0.01)0.0; (d) Ra=1(-0.052(0.01)0.0.[1]

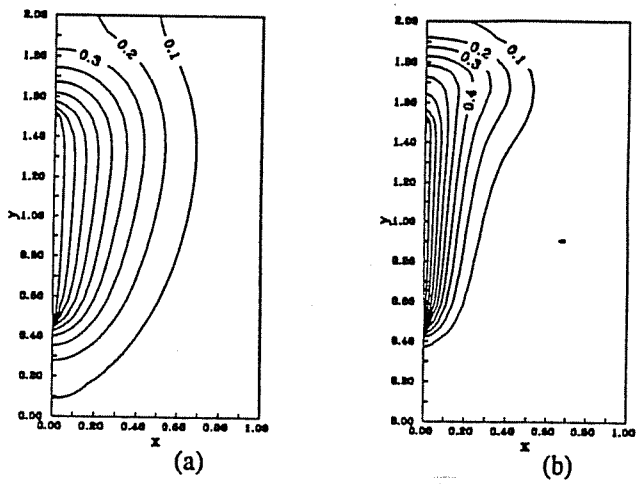

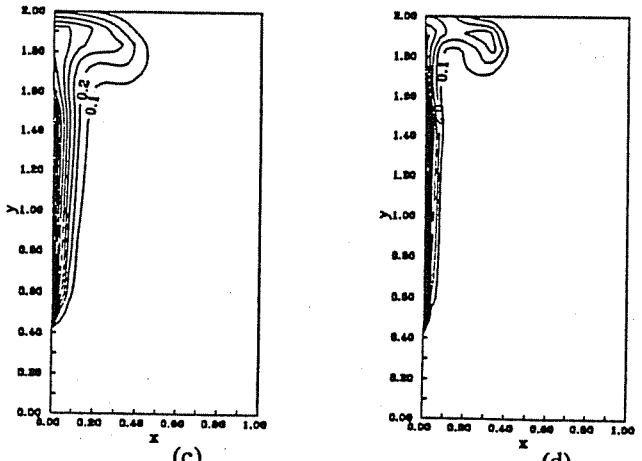

Fig. 14 : Contour maps of temperature at t^*=5.0: (a) Ra=10^3, $T_{min} = 0.1$, $\Delta T = 0.1$, $T_{max} = 1.0$ i.e., 0.1(0.1)1.0; (b) Ra=10^4, 0.1(0.1)1.0; (c) Ra=10^5, 0.1(0.1)1.0; (d) Ra=10^6, 0.1(0.1)1.0.

1 The stream function ψ is defined by $u = \partial\psi/\partial y$, $v = -\partial\psi/\partial x$. This definitio generates a contour which is everywhere tangent to the local velocity vector. Th change in stream function is an exact differential given by $\Delta\psi = \int(V \cdot n)d\Gamma$ wher V is the velocity vector and Γ is a general path of integration.

Table 4 includes the CPU times required for carrying the computations to a point in time such that the average temperature in the cavity is 97% of the plate temperature. (All computations are performed on an 8-CPU Cray YMP computer.)

Ra	CPU Time (sec)
10^3	685
10^4	922
10^5	1105
10^6	2190

Table 4 : CPU time required for cavity bulk temperature to reach 97% of T_w, 740 element mesh, $\gamma = 0.0001$.

5 Conclusions

A square cavity enclosing a heated isothermal vertical flat plate has been proposed as a suitable geometry for validating codes capable of computing solutions to time dependent Navier-Stokes and energy equations. Solutions are obtained over the Rayleigh number range $10^3 \le Ra \le 10^6$. Spatial and temporal refinement was performed to assure the computed benchmark solutions are mesh independent.

Acknowledgements

This work has been supported by the Solar Applications for Buildings, Conservation and Renewable Energy Division, U.S. Department of Energy. Computational resources have been provided by the San Diego Supercomputer Center.

Appendix A

The norm $\|E^j_{k+1}\|$ $(j = u, v, T)$ is defined based on the truncation error as given by Eq. 13.

$$E^j_{k+1} = \frac{j^c_{k+1} - j^p_{k+1}}{3\left(1 + \frac{\delta t_{k-1}}{\delta t_k}\right)} + O(\delta t_k^4)$$

Since the order of magnitude for each variable may differ considerably, the error is approximated by defining a relative norm.

$$\|E_{k+1}\| = \left\{ \frac{1}{N_u + N_v + N_T} \left[\sum_{i=1}^{N_u} \left(\frac{E^{u_i}_{k+1}}{|u^i_{k+1}|} \right)^2 + \sum_{i=1}^{N_v} \left(\frac{E^{v_i}_{k+1}}{|v^i_{k+1}|} \right)^2 + \sum_{i=1}^{T} \left(\frac{E^{T_i}_{k+1}}{|T^i_{k+1}|} \right)^2 \right] \right\}^{1/2}$$

where N_u, N_v, N_T are the respective number of free u-velocity, v-velocity, and temperature components.

Appendix B

As a supplement to Figs. 12-15, tabular results of v, u, T, and ψ at time t^*=5.0 for three locations in the cavity are given in Tables B1-B3. The time t^*=5.0 was selected because it is the time when velocities in the cavity are approaching their temporal maximums. The positions in the cavity selected for tabulating the results are regions with relatively high velocities or high gradients in the dependent variables. Linear interpolation is used when the quantities are not known at time t^*=5.0 or the three x-y locations.

Ra	u^*	v^*	ϕ	T
10^3	0.0	0.03888	0.0	0.3909
10^4	0.0	0.1405	0.0	0.5751
10^5	0.0	0.3588	0.0	0.6126
10^6	0.0	0.5379	0.0	0.5783

Table B1: Variable data at t^*=5.0, x^*=0.0, y^*=1.75.

Ra	u^*	v^*	ϕ	T
10^3	0.05015	0.02962	-0.009171	0.3021
10^4	0.1358	0.07178	-0.02936	0.3669
10^5	0.1480	0.04847	-0.05489	0.2072
10^6	0.04349	-0.007634	-0.05391	0.1624

Table B2: Variable data at t^*=5.0, x^*=0.25, y^*=1.75.

Ra	u^*	v^*	ϕ	T
10^3	0.06848	-0.00890	-0.01182	0.1504
10^4	0.1593	-0.05447	-0.03037	0.1056
10^5	0.1462	-0.1481	-0.03663	0.03963
10^6	0.06211	-0.1211	-0.02227	0.000399

Table B3: Variable data at t^*=5.0, x^*=0.50, y^*=1.75.

References

[1] Jones, I. P., "A Comparison Problem for Numerical Methods in Fluid Dynamics: The Double-Glazing Problem", *Numerical Methods in Thermal Problems* (edited by R. W. Lewis and K. Morgan), pp. 338-348, Pineridge Press, Swansen, U.K., (1979).

[2] de Vahl Davis, G., Jones, I. P., "Natural Convection in a Square Cavity: A Comparison Exercise", *International Journal for Numerical Methods in Fluids*, **3**, pp. 227-248 (1983).

[3] de Vahl Davis, G., "Natural Convection of Air in a Square Cavity: A Benchmark Numerical Solution", *International Journal for Numerical Methods in Fluids*, **3**, pp. 249-264 (1983).

[4] Khalilollahi, A., Sammakia, B., "Unsteady Natural Convection Generated by a Heated Surface Within an Enclosure", *Numerical Heat Transfer*, **9**, pp. 715-730, (1986).

[5] Gray, D. D., Giorgini, A., "The Validity of The Boussinesq Approximation fro Liquids and Gases", *International Journal of Heat and Mass Transfer*, **19**, pp. 545-551, (1976).

[6] FIDAP, A fluid dynamics analysis package by Fluid Dynamics International, Inc. 500 Davis St. Suite 600, Evanston, IL, 60201.

[7] Sani, R. L., Gresho, P. M., Lee, R. L., Griffiths, D. F., "The Cause and Cure(?) of the Spurious Pressures Generated by Certain GFEM Solutions of the Navier-Stokes Equations", *International Journal for Numerical Methods in Fluids*, **1**, pp. 17 (1981).

[8] Churchill, S. W., Chu, H. H. S., "Correlating Equations for Laminar and Turbulent Free Convection from a Vertical Plate", *International Journal of Heat and Mass Transfer*, **18** pp. 1323. (1975).